Materials Horizons

ROYAL SOCIETY OF CHEMISTRY

COMMUNICATION

View Article Online
View Journal

Cite this: DOI: 10.1039/d2mh00695b

Received 3rd June 2022,
Accepted 31st August 2022

DOI: 10.1039/d2mh00695b

rsc.li/materials-horizons

On-demand, remote and lossless manipulation of biofluid droplets†

Wei Wang, ‡[ab] Jiefeng Sun, ‡[c] Sravanthi Vallabhuneni, ‡[a] Benjamin Pawlowski,[c] Hamed Vahabi,[c] Kimberly Nellenbach,[de] Ashley C. Brown, [de] Frank Scholle,[f] Jianguo Zhao *[c] and Arun K. Kota *[a]

The recent global outbreaks of epidemics and pandemics have shown us that we are severely under-prepared to cope with infectious agents. Exposure to infectious agents present in biofluids (e.g., blood, saliva, urine etc.) poses a severe risk to clinical laboratory personnel and healthcare workers, resulting in hundreds of millions of hospital-acquired and laboratory-acquired infections annually. Novel technologies that can minimize human exposure through remote and automated handling of infectious biofluids will mitigate such risk. In this work, we present biofluid manipulators, which allow on-demand, remote and lossless manipulation of virtually any liquid droplet. Our manipulators are designed by integrating thermo-responsive soft actuators with superomniphobic surfaces. Utilizing our manipulators, we demonstrate on-demand, remote and lossless manipulation of biofluid droplets. We envision that our biofluid manipulators will not only reduce manual operations and minimize exposure to infectious agents, but also pave the way for developing inexpensive, simple and portable robotic systems, which can allow point-of-care operations, particularly in developing nations.

New concepts

Healthcare-associated infections pose a severe risk for healthcare workers and clinical laboratory personnel, who act as our first line of defense during epidemics and pandemics. Infectious agents present in biofluids result in hundreds of millions of hospital-acquired and laboratory-acquired infections each year. To minimize the exposure of healthcare workers and clinical laboratory personnel, we need novel techniques for on-demand, remote and lossless handling of infectious biofluid specimens in clinical settings. In this work, for the first time, we demonstrate on-demand, remote and lossless manipulation of biofluid droplets using soft actuators. We designed our biofluid manipulators by combining thermo-responsive soft actuators with superomniphobic surfaces. We demonstrate both in-plane manipulation (e.g., simultaneous and sequential transport) and out-of-plane manipulation (e.g., grip and release operations) to show the potential of our manipulators for automation. Furthermore, we demonstrate on-demand, remote and lossless manipulation of biofluid droplets to show the relevance of our manipulators for biomedical and biological applications. We envision that our biofluid manipulators will not only reduce manual operations and minimize exposure to infectious agents, but also pave the way for developing inexpensive, simple and portable robotic systems, which can allow point-of-care operations, particularly in developing nations.

Introduction

Exposure to infectious agents (e.g., pathogens like bacteria, viruses etc.) present in non-Newtonian or active biofluids (e.g., blood, saliva, urine etc.) poses a severe risk to clinical laboratory personnel and healthcare workers,[1–3] resulting in hundreds of millions of hospital-acquired and laboratory-acquired infections each year.[1,4–6] The recent global outbreaks of epidemics and pandemics (e.g., HIV/AIDS, MERS-CoV, Ebola, SARS-CoV-2 etc.) and the increased exposure of clinical laboratory personnel and healthcare workers to the highly infectious specimens, further emphasizes this risk. Novel technologies that can mitigate such risk by reducing manual operations and minimizing exposure time through remote and automated handling of infectious biofluids are indispensable.[7,8] In this work, we present biofluid manipulators, which allow on-demand, remote and lossless manipulation of a wide range of liquids, including biofluids (e.g., blood). Our biofluid manipulators are designed by integrating thermo-responsive soft

[a] Department of Mechanical and Aerospace Engineering, North Carolina State University, Raleigh, NC, 27695, USA. E-mail: akota2@ncsu.edu
[b] Department of Mechanical, Aerospace, and Biomedical Engineering, University of Tennessee, Knoxville, TN, 37996, USA
[c] Department of Mechanical Engineering, Colorado State University, Fort Collins, CO, 80523, USA. E-mail: jianguo.zhao@colostate.edu
[d] Joint Department of Biomedical Engineering, North Carolina State University and The University of North Carolina at Chapel Hill, Raleigh, NC, 27695, USA
[e] Comparative Medicine Institute, North Carolina State University, Raleigh, NC, 27695, USA
[f] Department of Biological Sciences, North Carolina State University, Raleigh, NC, 27695, USA
† Electronic supplementary information (ESI) available. See DOI: https://doi.org/10.1039/d2mh00695b
‡ These authors contributed equally to this work.

actuators with superomniphobic surfaces (i.e., surfaces that are extremely repellent to virtually all liquids) through a simple and versatile multi-layer design. While prior reports have engineered soft manipulators that can maneuver solid objects,[9–11] there are no reports of soft manipulators that can maneuver biofluid droplets. Furthermore, while there are several reports on droplet manipulation methods (e.g., electric fields, magnetic fields, light, heat, guiding tracks, and surface patterning),[12–17] they suffer from one or more of the following shortcomings – liquid loss or single-use or in-plane movement only or expensive fabrication or non-portable or not on-demand. Utilizing our biofluid manipulators, we overcome these shortcomings and demonstrate in-plane (simultaneous and sequential) transport and mixing of liquid droplets, as well as out-of-plane grip, transport and release of liquid droplets. While simultaneous in-plane manipulation of droplets enables automation of simple single-step processes, sequential in-plane manipulation enables automation of multi-step processes, which involve sequential mixing of droplets at different time intervals. The out-of-plane manipulation enables automation of more sophisticated processes that require pickup, transport and release of droplets across hurdles or obstacles on the surface. Furthermore, to illustrate the practical utility of our manipulators, we demonstrate on-demand, remote and lossless manipulation of biofluid droplets, including blood and virus replicons. We envision that our biofluid manipulators will not only reduce manual operations and minimize exposure to infectious agents, but also pave the way for developing inexpensive, simple and portable robotic systems, which can allow point-of-care operations, particularly in developing nations.

Results and discussion

In this work, to achieve on-demand and remote manipulation of liquid droplets, we fabricated manipulators by embedding a heterochiral twisted and coiled actuator (TCA)[18–20] between softer and stiffer elastomer layers (Fig. 1a–c). We used a heterochiral TCA because it can be easily fabricated with commercially available materials, it can be remotely actuated (i.e., elongated due to thermally induced untwisting) on-demand by Joule heating with a low voltage (3 V; Fig. 1a), it does not require additional bulky hardware, and it generates appreciable and reversible elongation,[18] which can generate considerable forces (about 100 times larger than a human muscle of same mass and length).[19] Our heterochiral TCA consisted of conductive nylon sewing threads twisted and coiled in opposite directions (see Experimental). We embedded a single heterochiral TCA (with a U shape) between a softer elastomer layer consisting of just a soft adhesive tape (Young's modulus of B104 kPa) and a stiffer elastomer layer consisting of the soft adhesive tape along with a stiffer tape (Young's modulus of B338 kPa; Fig. 1b and c). We used softer and stiffer elastomer layers because the softer side exhibits larger elongation than the stiffer side upon actuation (i.e., Joule heating with a voltage) of the heterochiral TCA. In order to accommodate this asymmetric elongation, the soft manipulator bends toward the stiffer side (Fig. 1d–f). Our soft manipulator can reversibly bend with large bending angles and recover quickly (Movie S1, ESI†). In order to characterize the actuation, we measured the output blocking force F_b (i.e., the force required to restrict further bending)[21–23] of the actuated soft manipulator (see Experimental). Our results indicate that the blocking force decreases with increasing bending curvature of the actuated soft manipulator (Fig. 1g). This is because at larger bending curvatures, the force generated by the actuated TCA is increasingly used to induce larger elastic deformations. However, even at a large bending curvature of B0.08 mm^{-1} (which is higher than the bending curvatures used in our experiments), the blocking force of our soft manipulator is B15 mN (sufficient to lift B1.5 g of liquid), which is more than an order of magnitude higher than the force required for handling millimeter-sized droplets of common liquids.

We also estimated the blocking force F_b at each bending curvature k by modeling the soft manipulator using a planar-elastica model[24] (see Section S1, ESI†). Assuming that there is a centerline passing through the soft manipulator body with an initial length L, we denote the arc length on this centerline by sA[0, L] with s = 0 and s = L representing the base and tip of the manipulator, respectively. We can then relate the blocking force F_b to the bending angle y(s) (relative to the vertical axis) of the manipulator using the force balance at arc length s:[24]

$$EI\frac{d^2y}{ds^2} = -F_b\cos(\theta(s) - \alpha) - F_{act}r\frac{dy}{ds} \quad (1)$$

Here E is the Young's modulus of the manipulator, I is the second moment of area for the manipulator cross section, a is the tip angle, r is the distance from the centerline to the TCA, and F_{act} is the actuation force generated by the TCA. Subsequently, we denote the position for the point located at s on the centerline as a two-dimensional vector p(s):

$$\frac{dp}{ds} = \begin{bmatrix} -\sin\theta(s) \\ \cos\theta(s) \end{bmatrix} \quad (2)$$

We can then obtain the manipulator's curvature k by fitting a circle to the base, middle, and tip points of the manipulator using the following equation:

$$k = \frac{4x_2^2(x_2y_3 - x_3y_3) - (x_3^2 + y_2^2)(x_2^2y_3 - x_3^2y_2 + y_2^2y_3 - y_2y_3^2)}{(x_2^2 + y_2^2)(x_2^2y_3 - x_3^2y_2 + y_2^2y_3 - y_2y_3^2)} \quad (3)$$

Here, x_2 and y_2 are the coordinates for the middle point $p_2 = p(L/2)$, and x_3 and y_3 are the coordinates for the tip point $p_3 = p(L)$. With eqn (1)–(3), and appropriate boundary conditions (see Section S1, ESI†), we estimated the blocking force F_b at a given curvature k. Our theoretical estimates matched well with our experimental measurements (Fig. 1g).

To design manipulators for lossless manipulation of liquid droplets, the adhesion between the liquid droplet and the surface of the manipulator should be minimized. One strategy for significantly reducing the adhesion is to fabricate manipulators with super-repellent surfaces.[25,26] Super-repellent

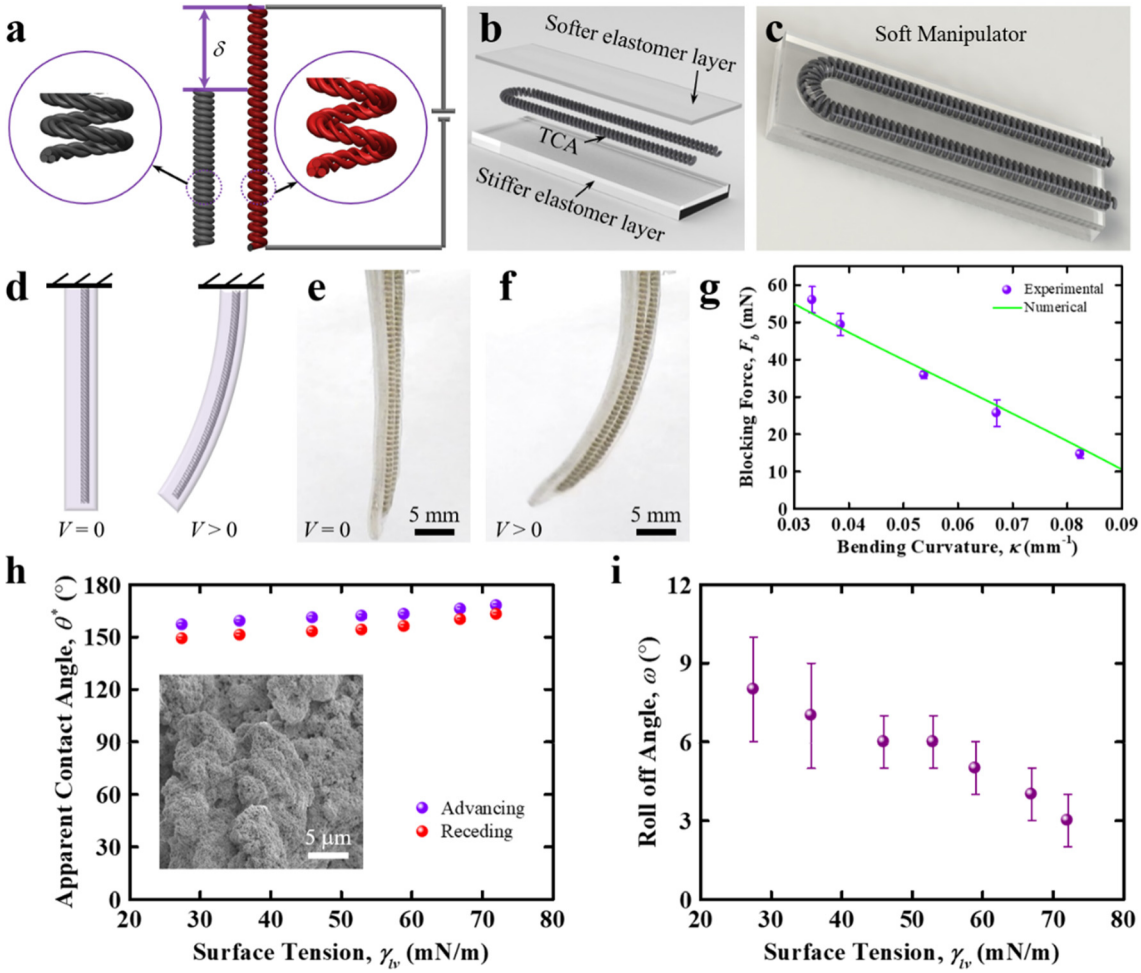

Fig. 1 Biofluid manipulator. (a) Schematic depicting the twisted-and-coiled actuator (TCA) fabricated with conductive nylon sewing thread. When a voltage is applied, the TCA extends in length. (b) Schematic illustrating the fabrication of soft manipulator by embedding a single heterochiral TCA between softer and stiffer elastomer layers. (c) Schematic depicting the soft manipulator after embedding a single TCA between the softer and stiffer elastomer layers. (d) Schematic depicts the bending process of our soft manipulator. (e and f) Pictures showing the bending of the soft manipulator when a voltage is applied. (g) Blocking force generated by the soft manipulator at different bending curvatures. (h and i) Apparent contact angles and roll off angles, respectively, of liquid droplets with different surface tensions on our superomniphobic surfaces. Roll off angles were measured with 20 mL droplets. The inset shows the morphology of our superomniphobic surfaces.

surfaces are broadly classified as superhydrophobic and superomniphobic. Superhydrophobic surfaces display extreme repellency (i.e., low adhesion) to aqueous liquids,[27] while superomniphobic surfaces display extreme repellency to virtually any liquid (aqueous or organic; acids, bases or solvents; Newtonian or non-Newtonian etc.).[28–32] Superomniphobic surfaces can be designed by combining materials possessing low solid surface energy with appropriate re-entrant surface texture (i.e., convex or overhang structures).[33–36] While low solid surface energy results in high contact angles, appropriate re-entrant surface texture results in a stable Cassie-Baxter state[37] for a wide range of liquids.[28,34,36] Manipulators with such superomniphobic surfaces can be used for lossless handling of a wide range of liquid droplets, including biofluids. So, we fabricated our biofluid manipulators by spray-coating fluorinated fumed silica particles on our soft manipulators (see Experimental). The spray coated fumed silica particle morphology provided the re-entrant structure (Fig. 1h) and the fluorination of these fumed silica particles provided the low solid surface energy, which together rendered the surface superomniphobic. To quantify the superomniphobicity, we measured the apparent advancing y_{adv} and apparent receding y_{rec} contact angles of a wide range of liquids with surface tensions ranging from 27.5 mN m^{ÿ1} to 72.1 mN m^{ÿ1} (Fig. 1h). All tested liquids displayed apparent contact angles y* Z 1501 and low contact angle hysteresis Dy ¼ y_{adv} ÿ y_{rec} on our superomniphobic surfaces. The low contact angle hysteresis led to high mobility (or low adhesion) of droplets, as evidenced by the low roll off angles o o 101 (Fig. 1i). The ultra-low liquid adhesion was also evident from the complete rebound of droplets upon impacting the superomniphobic surfaces (Movie S2, ESI†). To quantify the lossless nature of our droplet manipulation and cross-contamination on our biofluid manipulator, we measured the droplet volume, actuator mass and droplet roll off angle as a function of droplet rastering cycles for a series of liquids (hexadecane, water, Bradford reagent, Bovine

Serum Albumin (BSA), milk, virus replicon particle laden solution, thrombin, whole blood, fibrinogen and platelet rich plasma (PRP)) on the same manipulator. Our results indicate that there is no change in the droplet volume or appearance, actuator mass or appearance and droplet roll off angle even after 1000 droplet rastering cycles with each liquid (see Section S3, ESI†). This confirms that there is neither liquid loss nor noticeable cross-contamination on our biofluid manipulators.

To demonstrate on-demand, remote and loss-less, in-plane manipulation of droplets with our biofluid manipulators, we designed two different manipulators – one for simultaneous manipulation of droplets and another for sequential manipulation of droplets. While simultaneous in-plane manipulation of droplets enables automation of simple single-step processes (e.g., colorimetric assays, where a single indicator is used to detect a single analyte), sequential in-plane manipulation enables automation of multi-step processes, which involve sequential mixing of droplets at different time intervals (e.g., colorimetric enzymatic assays, where multiple indicators are utilized to detect a single/multiple analytes that require sequential droplet manipulation). For simultaneous manipulation of droplets, our design consisted of a single heterochiral TCA in an elliptical shape with the stiffer elastomer layer facing upward (Fig. S2, ESI†) such that the two free ends of manipulator can bend upward simultaneously upon actuation. The manipulator was rendered superomniphobic by spray coating with fluorinated fumed silica particles. To demonstrate simultaneous manipulation of droplets, we placed two 25 mL water droplets (dyed red and blue) close to the free ends of the manipulator (initially horizontal; Fig. 2a). Then, we actuated the manipulator to initiate its bending upward. When the tilt exceeded the roll off angle o, the red and blue water droplets rolled simultaneously along the manipulator surface and mixed with each other (Fig. 2b and Movie S3, ESI†). In addition to handling high surface tension aqueous droplets, our manipulator allows handling of a wide variety of low surface tension droplets, as evident from simultaneous manipulation and mixing of two n-hexadecane droplets (colorless and dyed red; Fig. 2c and d, and Movie S4, ESI†). For sequential manipulation of droplets, our design consisted of three manipulators that can be actuated independently (Fig. 2e). The three manipulators were arranged around a triangular-shaped domain. While the manipulators were rendered superomniphobic by spray coating with fluorinated fumed silica particles, the triangular-shaped domain was not super-repellent. In other words, liquid droplets displayed low adhesion on the biofluid manipulators and high adhesion on the triangular-shaped domain. This allowed the triangular-shaped domain to act as a site that traps droplets and enables interactions (e.g., mixing, reaction etc.). To demonstrate sequential manipulation of droplets, we placed three 25 mL water droplets (dyed in red, yellow and blue) close to the free end of each of the three manipulators (initially horizontal, Fig. 2f). Then, we actuated one of the manipulators (with the red water droplet) to initiate its bending. When the tilt exceeded the roll off angle o, the red water droplet rolled down under gravity, along the manipulator surface and got trapped in the triangular-shaped domain (Fig. 2g and Movie S5, ESI†). Upon actuation of the second manipulator (with the yellow water droplet), the yellow water droplet rolled down and mixed with the red droplet in the triangular-shaped domain (Fig. 2h). Similarly, actuation of the third manipulator (with the blue water droplet) allowed the blue water droplet to roll down and mix with the droplet in the triangular-shaped domain (Fig. 2i). In this manner, droplets can be sequentially or simultaneously transported and mixed on-demand in a lossless manner with our manipulators.

To demonstrate on-demand, remote and lossless, out-of-plane manipulation of droplets with our manipulators, we designed a droplet gripper consisting of two vertical manipulators with folded stainless steel meshes attached to the free ends (Fig. 3a). All manipulator surfaces were rendered superomniphobic by spray coating with fluorinated fumed silica particles. Two manipulators were aligned such that the stiffer elastomer layers faced each other so that the manipulators can bend towards each other upon actuation to initiate gripping action. The folded stainless steel meshes (similar to a ladle) provided the geometric constraint necessary to prevent undesired slip of the liquid droplets during the controlled pickup and release operations. When the two manipulators were actuated by applying 3 V, the asymmetric elongation induced by Joule heating caused them to bend towards each other and the distance between them decreased until they came in contact with each other (Fig. 3b). When the voltage was turned off (i.e., 0 V), the two superomniphobic manipulators recovered their original shapes (Fig. 3c). Utilizing our droplet gripper, we could generate sufficient force to hold a 3.6 g droplet of gallium–indium liquid metal (Fig. 3d). Furthermore, utilizing our droplet gripper, we performed pick-and-place operations (i.e., droplets were gripped, lifted, transported, and released) to demonstrate out-of-plane droplet manipulation. Our droplet gripper can enable pick-and-place operations for a wide variety of liquid droplets. To demonstrate this, we placed two 40 mL droplets of water (a representative high surface tension liquid; one droplet dyed blue and another dyed yellow) on a superomniphobic surface (Fig. 3e). The droplet gripper was initially positioned above the blue water droplet. Using a translation stage, the droplet gripper was descended. Upon approaching the droplet, we actuated the two manipulators so that blue water droplet could be gripped (i.e., picked up out-of-plane from the surface) on-demand. Subsequently, using the translation stage, the blue water droplet was lifted, transported in the horizontal direction until it is positioned above the yellow water droplet, and then descended (Fig. 3f and Movie S6, ESI†). Subsequently, the voltage was turned off so that the blue droplet could be released (out-of-plane) on-demand, in a lossless manner (due to the low adhesion of the superomniphobic surfaces) and mixed with the yellow droplet (Fig. 3g). In addition to high surface tension aqueous droplets, our manipulators can also be used to perform on-demand and lossless pick-and-place operations with low surface tension liquid droplets. To demonstrate this, an n-hexadecane droplet dyed red was gripped, lifted, transported, and released on a colorless

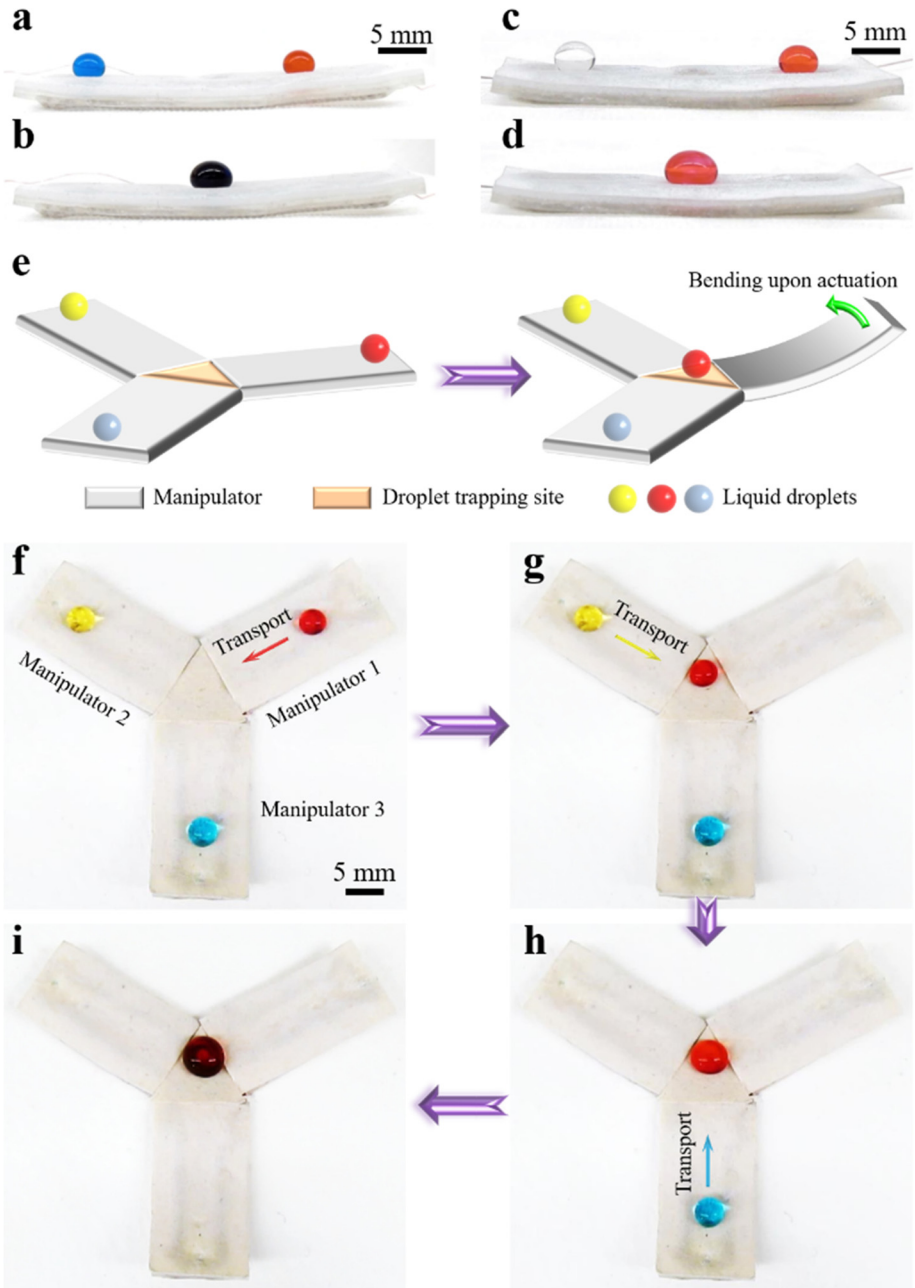

Fig. 2 Manipulators for in-plane droplet manipulations. (a and b) and (c and d) On-demand, remote and lossless, in-plane simultaneous manipulation of water droplets (dyed blue and red) and n-hexadecane droplets (colorless and dyed red), respectively, with our biofluid manipulator. Upon actuation, the two droplets are transported simultaneously along the surface and mixed with each other. (e) Schematic depicting the design of three manipulators for in-plane sequential manipulation of droplets. Each manipulator can be actuated independently. (f–i) On-demand, remote and loss-less, in-plane sequential manipulation of water droplets. Upon actuation, each droplet is sequentially transported to the trapping site (i.e., triangular-shaped domain).

n-hexadecane droplet (Fig. 3h–j, and Movie S7, ESI†). In this manner, droplets can be transported out-of-plane and mixed on-demand in a lossless manner with our manipulators. Due to the simplicity and versatility of our design, it is easy to fabricate a large array of manipulators for in-plane (i.e., simultaneous and sequential) and out-of-plane manipulations of multiple droplets and incorporate them into inexpensive, simple and potable robotic systems for point-of-care operations.

In order to illustrate the practical utility of our manipulators in reducing the exposure of clinical laboratory personnel and healthcare workers to infectious specimens, we demonstrate on-demand, remote and lossless manipulation of biofluid droplets. While maneuvering of solids has been reported in prior studies,[38,39] to the best of our knowledge, on-demand, remote and lossless handling of biofluid droplets has never been demonstrated. Here, we demonstrate a simple in-plane

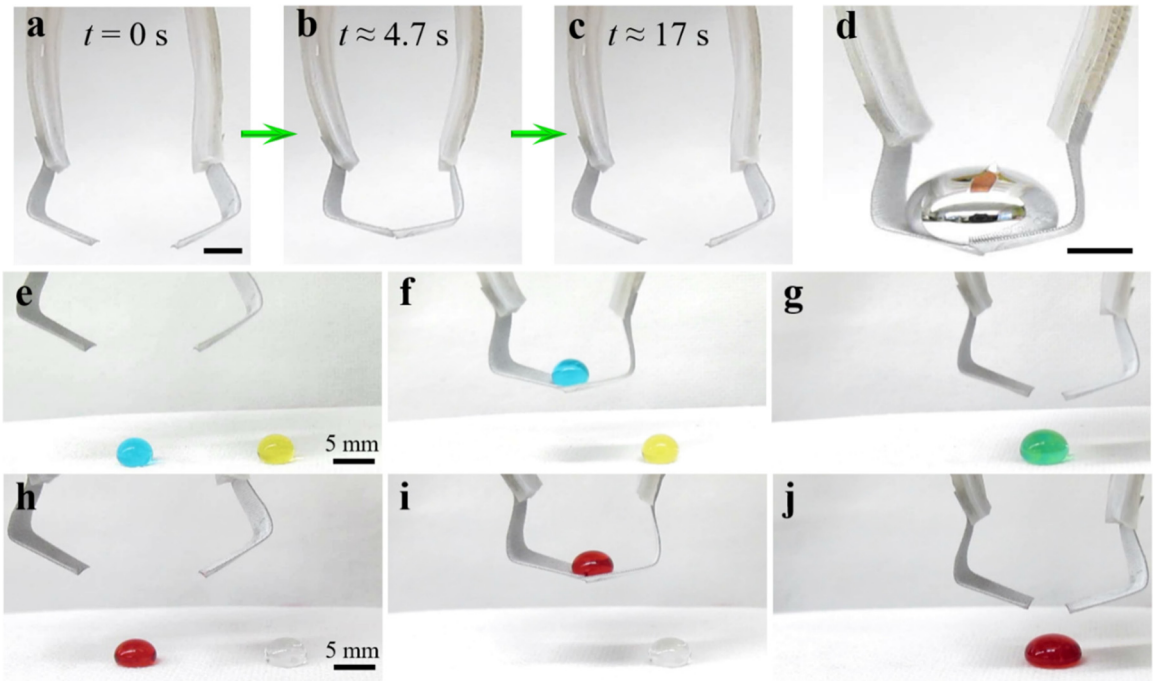

Fig. 3 Droplet gripper. (a–c) Droplet gripper consisting of two manipulators. When the voltage was applied, distance between the manipulators decreased until they contacted each other. When the voltage was turned off, the gripper recovered its original shape. Scale bar represents 5 mm. (d) The droplet gripper holding a 3.6 g gallium–indium liquid metal droplet. Scale bar represents 5 mm. (e–g) and (h–j) On demand, remote and lossless, pick-and-place operations (i.e., out-of-plane manipulation) of water droplets (dyed blue and yellow) and n-hexadecane droplets (colorless and dyed red), respectively.

simultaneous manipulation of biofluid droplets relevant to biological assays (e.g., colorimetric assays and blood coagulation assays). For colorimetric assays, we demonstrate protein detection with Bradford reagent (Coomassie Blue G-250 dye). We placed 30 mL droplets of Bradford reagent (reddish brown) and liquids containing proteins (BSA, Fig. 4a–c; milk, Fig. 4d–f; virus replicon particle-laden solution, Fig. 4g–i) on the free ends of our manipulators. Upon actuation, the droplets on either end rolled past the surface and started mixing with each other at the center of the manipulator (Fig. 4b, e and h). While mixing, the droplets displayed a color change to blue, indicating the presence of proteins (Fig. 4c, f and i, and Movies S8–S10, ESI†). This is because Bradford reagent forms a dye-protein complex, which leads to a shift in its absorption wavelength from E470 nm to E595 nm.[40–42] In this manner, our biofluid manipulators can be used to detect the presence of proteins in a wide range of biofluids commonly used in clinical settings. For blood coagulation assays, we demonstrate clotting of whole blood and blood components (e.g., PRP and fibrinogen) using thrombin. We placed 30 mL droplets of thrombin (colorless) and whole blood (red; Fig. 4j), PRP (cloudy; Fig. 4m) and fibrinogen (colorless; Fig. 4p) on the free ends of our biofluid manipulators. Upon actuation, the droplets on either side rolled past the surface and merged with each other at the center of the manipulator (Fig. 4k, n and q). After merging with thrombin, the viscosity of whole blood, PRP and fibrinogen gradually increased to transition from a liquid to a gel, indicating clot formation within the droplets (Fig. 4l, o and r, and Movies S11–S13, ESI†). This is because thrombin, a serine protease, cleaves fibrinogen (a soluble coagulation protein present in blood plasma) into fibrin monomers, which further polymerize to form a fibrous network resulting in gelation/clotting.[43–45] In this manner, our biofluid manipulators can be used to study the clotting kinetics using very small quantities of blood and blood components. While we demonstrated protein detection and blood coagulation qualitatively using our biofluid manipulators, the relevant quantitative parameters (e.g., protein, analyte or pathogen concentration in colorimetric assays and clotting time or coagulation factor in blood coagulation assays) can also be determined easily in conjunction with optical techniques (e.g., spectrophotometry, turbidometry etc.). Furthermore, unlike superhydrophobicity, superomniphobicity of our manipulators allows droplet manipulation for a wide range of biofluids (water-based and lipid-based). Thus, on-demand, remote and lossless manipulation of wide range of biofluids (e.g., blood, saliva, urine etc.) can be performed utilizing our biofluid manipulators, thereby reducing the exposure of clinical laboratory personnel and healthcare workers to infectious specimens, especially during pandemics.

Conclusions

In summary, we developed biofluid manipulators, by combining twisted-and-coiled actuators embedded in a soft body with superomniphobic surfaces. Utilizing our manipulators, we

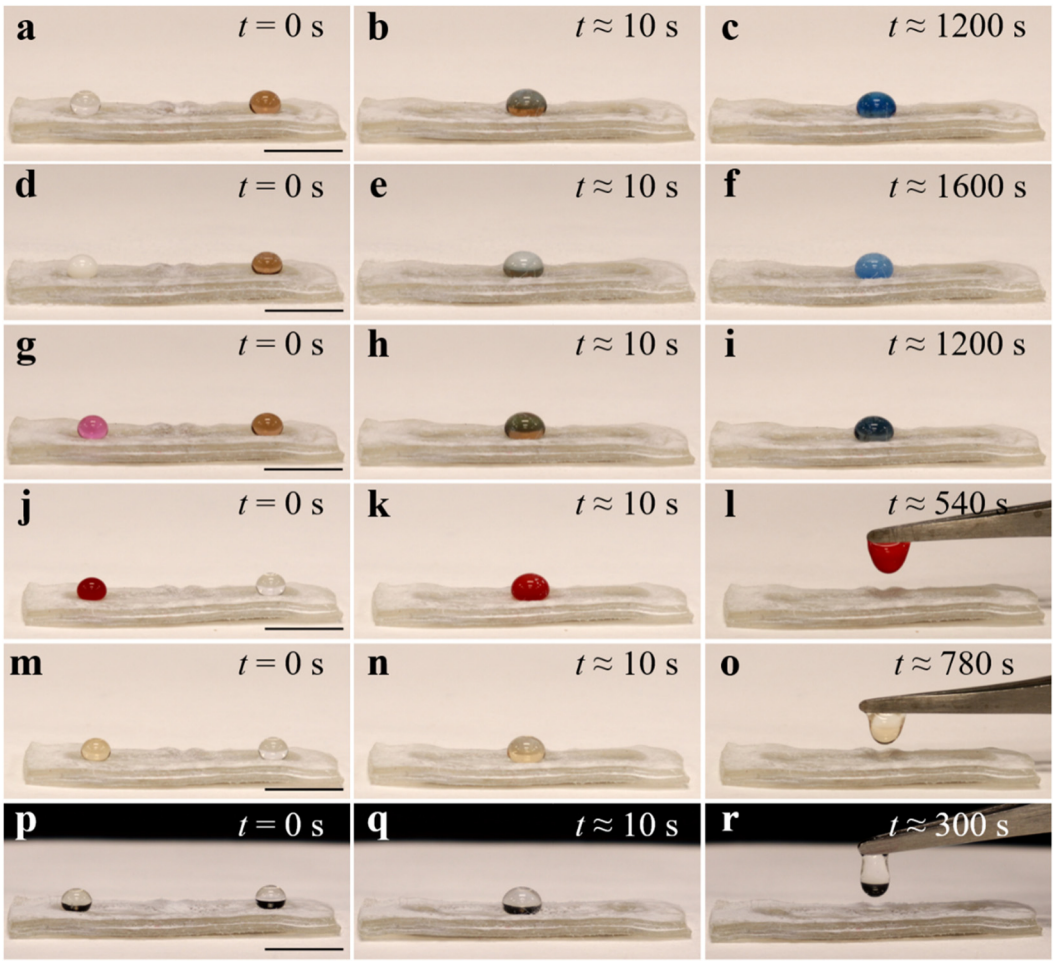

Fig. 4 Biofluid droplet manipulation. (a–c), (d–f) and (g–i) On-demand, remote and lossless in-plane simultaneous mixing of BSA, milk and virus replicon particle-laden droplets, respectively, with Bradford reagent (right; reddish brown) to demonstrate protein detection. (j–l), (m–o) and (p–r) On-demand, remote and lossless in-plane simultaneous mixing of whole blood, PRP and fibrinogen droplets, respectively, with thrombin (right) to demonstrate clotting. Scale bar represents 10 mm.

demonstrated on-demand, remote and lossless manipulation of high surface tension and low surface tension liquid droplets, both in-plane (e.g., simultaneous and sequential transport) and out-of-plane (e.g., pickup and release). Furthermore, we demonstrated on-demand, remote and lossless manipulation of biofluid droplets to illustrate the utility of our manipulators in biological assays (e.g., colorimetric assays and blood coagulation assays). We envision that our biofluid manipulators will not only reduce manual operations and minimize exposure to infectious agents, but also pave the way for developing inexpensive, simple and portable robotic systems, which can allow point-of-care operations, particularly in developing nations.

Experimental

Fabrication of heterochiral twisted-and-coiled actuators (TCAs)

The heterochiral TCAs were fabricated with silver coated nylon sewing threads (Shieldex Trading, 235/35 4ply). Two nylon threads were first twisted together by generating twists from one end of the thread with a step motor, while exerting a load of 380 g on the other end of the thread. The twisted nylon threads were then coiled around a copper wire with a diameter of 0.4 mm using a custom-built apparatus. The opposite directions of coiling and twisting resulted in the heterochiral TCAs. Subsequently, the TCAs were annealed at 180 1C for 1 hour in an oven (Quincy Lab, 10GCE) to stabilize the structure of the TCAs. The copper wire was removed after the TCAs were cooled down to room temperature.

Fabrication of biofluid manipulators

A TCA arranged in a U shape (for droplet gripper and sequential droplet manipulation) or an elliptical shape (for simultaneous droplet manipulation) was sandwiched between two layers of soft adhesive tape (3M Inc., VHB tape 4905). To create asymmetric stiffness, a soft elastomer layer fabricated by folding a self-fusing silicone tape (Loctite Inc., Go2 wrap) was attached to one side of the soft body. The two ends of the TCA were connected to copper wires that acted as electrical leads. The surface of the manipulator was rendered superomniphobic by spray-coating with fluorinated fumed silica particles.

The fluorinated particles were fabricated through liquid phase silanization of 500 mg of 7 nm fumed silica particles (Sigma-Aldrich) in 20 mL hexane containing 0.5 mL heptadecafluoro-1,1,2,2-tetrahydrodecyl trichlorosilane (Gelest Inc.) for three days. Our biofluid manipulators can easily handle liquid volumes from 5 mL to 5 mL.

Measurement of blocking force

The blocking force generated by the manipulator at each bending curvature was measured by placing the probe of a force gauge (M3-012, Mark-10 Inc.) in the bending path of the manipulator. The probe was positioned to ensure that it contacted the tip of the manipulator. Three measurements were performed for each bending curvature.

Characterization of surface morphology

The morphology of the superomniphobic surface was characterized using a scanning electron microscope (JEOL JSM-6500F) at 10 kV.

Measurement of contact angles

The apparent advancing and receding contact angles as well as the roll off angles of liquids with a wide range of surface tensions were measured using a contact angle goniometer (Ramé-Hart 200-F1). For each liquid, three measurements were performed.

Preparation of Biofluids

Bovine serum albumin (BSA) droplets were prepared by diluting BSA (2 mg $mL^{\ddot{y}1}$; Fisher Scientific) to 2 ng $mL^{\ddot{y}1}$ with water. Virus replicon particle-laden droplets were prepared by suspending virus in 10% fetal bovine serum (FBS) buffer. Instead of using infectious virus, for safety reasons, we chose to use single-cycle infectious virus replicon particles (VRPs). To produce VRPs, a trans-packaging system for WNV replicons was used. Briefly, a BHK packaging cell line (VEEV-WNV C-E-Pac) harboring a Venezuelan Encephalitis virus replicon expressing the structural coding region of WNV (VEEV-WNV C-E-Pac)[46] was infected with previously produced WNV replicon particles, whose genome contains a deletion in the capsid protein C coding region. These replicon particles are able to infect regular cells, but due to the mutation in the C protein, they are not able to package their genome and produce progeny particles after the initial infection (single cycle infectious particles). However, full-length C protein expressed from VEEV-WNV C-E-Pac in the packaging cell line complements the defective C protein in the WNV replicon, leading to packaging of replicon genomes and secretion of WNV VRPs.[47] VRPs were produced in Dulbecco's Modified Eagle medium (DMEM), supplemented with antibiotics and 10% FBS. Whole blood (porcine) obtained from two-year-old female swine from North Carolina State University's tissue sharing program. Plasma was separated from blood by centrifugation twice at 15 000 g for 15 min. Thrombin droplets were prepared by diluting thrombin (100 mg $mL^{\ddot{y}1}$, Enzyme Research Laboratories) to 20 mg $mL^{\ddot{y}1}$. Fibrinogen droplets were prepared by diluting fibrinogen (20 mg $mL^{\ddot{y}1}$, Fib3 Fibrinogen with fibronectin, von Willebrand Factor, and Factor XIII depleted, Enzyme Research Laboratories) to 3 mg $mL^{\ddot{y}1}$.

Author contributions

Wei Wang, Jianguo Zhao and Arun K. Kota conceived the idea. Wei Wang, Jiefeng Sun, Sravanthi Vallabhuneni, Kimberly Nellenbach, Frank Scholle, and Hamed Vahabi conducted experiments. Benjamin Pawlowski conducted numerical simulations. Wei Wang, Jiefeng Sun, Sravanthi Vallabhuneni, Jianguo Zhao, Arun K. Kota conducted the analysis. Wei Wang, Jiefeng Sun, Sravanthi Vallabhuneni, Ben Pawlowski, Hamed Vahabi, Kimberly Nellenbach, Ashley C. Brown, Frank Scholle, Jianguo Zhao, Arun K. Kota wrote the manuscript.

Conflicts of interest

There are no conflicts to declare.

Acknowledgements

Arun K. Kota gratefully acknowledges financial support under award 1751628 from the National Science Foundation and under awards R01HL135505 and R21HL139208 from the National Institutes of Health. Jianguo Zhao gratefully acknowledges financial support under award 1755766 from the National Science Foundation. Frank Scholle gratefully acknowledges support from the Comparative Medicine Institute, North Carolina State University.

References

1 R. A. Weinstein and K. Singh, Laboratory-acquired infections, Clin. Infect. Dis., 2009, 49(1), 142–147.
2 D. L. Sewell, Laboratory-associated infections and biosafety, Clin. Microbiol. Rev., 1995, 8(3), 389–405.
3 A. Nienhaus, C. Kesavachandran, D. Wendeler, F. Haamann and M. Dulon, Infectious diseases in healthcare workers–an analysis of the standardised data set of a German compensation board, J. Occup. Med. Toxicol., 2012, 7(1), 8.
4 R. M. Pike, Laboratory-associated infections: incidence, fatalities, causes, and prevention, Annu. Rev. Microbiol., 1979, 33(1), 41–66.
5 W. H. Organization, Health care-associated infections fact sheet, World Health Organization, 2015, p. 4.
6 M. Haque, M. Sartelli, J. McKimm and M. A. Bakar, Health care-associated infections–an overview, Infect. Drug Resist., 2018, 11, 2321.
7 K. W. Miller, N. Grossman, P. Haviernik, J. Wolff, C.-L. Fu, B. Bare and E. Sindelar, A Semi-Automated Tuberculosis Testing Workflow Reduces Manual Hazardous Sample Handling and Hands-On Time: A Proof-of-Concept Study, SLAS Technol., 2019, 2472630319884519.
8 J. Ince and A. McNally, Development of rapid, automated diagnostics for infectious disease: advances and challenges, Expert Rev. Med. Devices, 2009, 6(6), 641–651.
9 D. Rus and M. T. Tolley, Design, fabrication and control of soft robots, Nature, 2015, 521(7553), 467–475.

10 H. Wang, M. Totaro and L. Beccai, Toward perceptive soft robots: Progress and challenges, Adv. Sci., 2018, 5(9), 1800541.
11 G. R. Gossweiler, C. L. Brown, G. B. Hewage, E. Sapiro-Gheiler, W. J. Trautman, G. W. Welshofer and S. L. Craig, Mechanochemically active soft robots, ACS Appl. Mater. Interfaces, 2015, 7(40), 22431–22435.
12 L. Sun, F. Bian, Y. Wang, Y. Wang, X. Zhang and Y. Zhao, Bioinspired programmable wettability arrays for droplets manipulation, Proc. Natl. Acad. Sci. U. S. A., 2020, 117(9), 4527–4532.
13 C. Liu, Y. Sun, J. Huanng, Z. Guo and W. Liu, External-field-induced directional droplet transport: A review, Adv. Colloid Interface Sci., 2021, 295, 102502.
14 W. Feng, E. Ueda and P. A. Levkin, Droplet Microarrays: From Surface Patterning to High-Throughput Applications, Adv. Mater., 2018, 30(20), 1706111.
15 R. Malinowski, I. P. Parkin and G. Volpe, Advances towards programmable droplet transport on solid surfaces and its applications, Chem. Soc. Rev., 2020, 49(22), 7879–7892.
16 S. Movafaghi, W. Wang, A. Metzger, D. Williams, J. Williams and A. K. Kota, Tunable superomniphobic surfaces for sorting droplets by surface tension, Lab Chip, 2016, 16(17), 3204–3209.
17 L. Zhu, C. Shao, H. Chen, Z. Chen and Y. Zhao, Hierarchical Hydrogels with Ordered Micro-Nano Structures for Cancer-on-a-Chip Construction, Research, 2021, 2021, 9845679.
18 C. S. Haines, N. Li, G. M. Spinks, A. E. Aliev, J. Di and R. H. Baughman, New twist on artificial muscles, Proc. Natl. Acad. Sci. U. S. A., 2016, 113(42), 11709–11716.
19 C. S. Haines, M. D. Lima, N. Li, G. M. Spinks, J. Foroughi, J. D. Madden, S. H. Kim, S. Fang, M. J. de Andrade and F. Göktepe, Artificial muscles from fishing line and sewing thread, Science, 2014, 343(6173), 868–872.
20 A. Abbas and J. Zhao, In Aphysics based model for twisted and coiled actuator, 2017 IEEE International Conference on Robotics and Automation (ICRA), IEEE, 2017, pp. 6121–6126.
21 X. Huang, K. Kumar, M. K. Jawed, A. Mohammadi Nasab, Z. Ye, W. Shan and C. Majidi, Highly Dynamic Shape Memory Alloy Actuator for Fast Moving Soft Robots, Adv. Mater. Technol., 2019, 1800540.
22 D. Trivedi, C. D. Rahn, W. M. Kier and I. D. Walker, Soft robotics: Biological inspiration, state of the art, and future research, Appl. Bionics Biomech., 2008, 5(3), 99–117.
23 A. D. Marchese, R. K. Katzschmann and D. Rus, A recipe for soft fluidic elastomer robots, Soft Robot., 2015, 2(1), 7–25.
24 S. P. Timoshenko and J. M. Gere, Theory of elastic stability, Courier Corporation, 2009.
25 J. Wang, W. Gao, H. Zhang, M. Zou, Y. Chen and Y. Zhao, Programmable wettability on photocontrolled graphene film, Sci. Adv., 2018, 4(9), eaat7392.
26 H. Zhang, G. Chen, Y. Yu, J. Guo, Q. Tan and Y. Zhao, Microfluidic printing of slippery textiles for medical drainage around wounds, Adv. Sci., 2020, 7(16), 2000789.
27 A. Lafuma and D. Quéré, Superhydrophobic states, Nat. Mater., 2003, 2(7), 457–460.
28 A. Tuteja, W. Choi, M. Ma, J. M. Mabry, S. A. Mazzella, G. C. Rutledge, G. H. McKinley and R. E. Cohen, Designing superoleophobic surfaces, Science, 2007, 318(5856), 1618–1622.
29 S. Pan, A. K. Kota, J. M. Mabry and A. Tuteja, Superomniphobic surfaces for effective chemical shielding, J. Am. Chem. Soc., 2012, 135(2), 578–581.
30 W. Wang, J. Salazar, H. Vahabi, A. Joshi-Imre, W. E. Voit and A. K. Kota, Metamorphic superomniphobic surfaces, Adv. Mater., 2017, 29(27), 1700295.
31 H. Vahabi, W. Wang, J. M. Mabry and A. K. Kota, Coalescence-induced jumping of droplets on superomniphobic surfaces with macrotexture, Sci. Adv., 2018, 4(11), eaau3488.
32 X. Deng, L. Mammen, H.-J. Butt and D. Vollmer, Candle soot as a template for a transparent robust superamphiphobic coating, Science, 2012, 335(6064), 67–70.
33 B. Su, Y. Tian and L. Jiang, Bioinspired interfaces with superwettability: from materials to chemistry, J. Am. Chem. Soc., 2016, 138(6), 1727–1748.
34 T. Darmanin and F. Guittard, Superhydrophobic and superoleophobic properties in nature, Mater. Today, 2015, 18(5), 273–285.
35 J. Yong, F. Chen, Q. Yang, J. Huo and X. Hou, Superoleophobic surfaces, Chem. Soc. Rev., 2017, 46(14), 4168–4217.
36 Z. Chu and S. Seeger, Superamphiphobic surfaces, Chem. Soc. Rev., 2014, 43(8), 2784–2798.
37 A. Cassie and S. Baxter, Wettability of porous surfaces, Trans. Faraday Soc., 1944, 40, 546–551.
38 E. Brown, N. Rodenberg, J. Amend, A. Mozeika, E. Steltz, M. R. Zakin, H. Lipson and H. M. Jaeger, Universal robotic gripper based on the jamming of granular material, Proc. Natl. Acad. Sci. U. S. A., 2010, 107(44), 18809–18814.
39 J. Shintake, V. Cacucciolo, D. Floreano and H. Shea, Soft Robotic Grippers, Adv. Mater., 2018, 30, 1707035.
40 C. V. Sapan, R. L. Lundblad and N. C. Price, Colorimetric protein assay techniques, Biotechnol. Appl. Biochem., 1999, 29(2), 99–108.
41 N. J. Kruger, The Bradford method for protein quantitation, Protein Protoc. Handb., 2009, 17–24.
42 S. J. Compton and C. G. Jones, Mechanism of dye response and interference in the Bradford protein assay, Anal. Biochem., 1985, 151(2), 369–374.
43 K. Göbel, S. Eichler, H. Wiendl, T. Chavakis, C. Kleinschnitz and S. G. Meuth, The coagulation factors fibrinogen, thrombin, and factor XII in inflammatory disorders—a systematic review, Front. immunol., 2018, 9, 1731.
44 T. Kawase, K. Okuda, L. F. Wolff and H. Yoshie, Platelet-rich plasma-derived fibrin clot formation stimulates collagen synthesis in periodontal ligament and osteoblastic cells in vitro, J. Periodontol., 2003, 74(6), 858–864.
45 V. Gubala, L. F. Harris, A. J. Ricco, M. X. Tan and D. E. Williams, Point of care diagnostics: status and future, Anal. Chem., 2012, 84(2), 487–515.
46 R. Fayzulin, F. Scholle, O. Petrakova, I. Frolov and P. W. Mason, Evaluation of replicative capacity and genetic stability of West Nile virus replicons using highly efficient packaging cell lines, Virology, 2006, 351(1), 196–209.
47 D. G. Widman, T. Ishikawa, E. R. Winkelmann, E. Infante, N. Bourne and P. W. Mason, RepliVAX WN, a single-cycle flavivirus vaccine to prevent West Nile disease, elicits durable protective immunity in hamsters, Vaccine, 2009, 27(41), 5550–5553.

Electronic Supplementary Material (ESI)

for

On-demand, Remote and Lossless Manipulation of Biofluid Droplets

Wei Wang,†[a] Jiefeng Sun,†[b] Sravanthi Vallabhuneni,†[a] Ben Pawlowski,[b] Hamed Vahabi,[b] Kimberly Nellenbach,[cd] Ashley C. Brown,[cd] Frank Scholle,[e] Jianguo Zhao,*[b] Arun K. Kota*[a]

a. *Department of Mechanical and Aerospace Engineering, North Carolina State University, Raleigh, NC 27695, USA. E-mail: akota2@ncsu.edu*

b. *Department of Mechanical Engineering, Colorado State University, Fort Collins, CO 80523, USA. E-mail: jianguo.zhao@colostate.edu*

c. *Joint Department of Biomedical Engineering, North Carolina State University and The University of North Carolina at Chapel Hill, Raleigh, NC 27695, USA.*

d. *Comparative Medicine Institute, North Carolina State University, Raleigh, NC 27695, USA.*

e. *Department of Biological Sciences, North Carolina State University, Raleigh, NC 27695, USA.*

† These authors contributed equally to this work.

*Corresponding authors: *jianguo.zhao@colostate.edu* and *akota2@ncsu.edu*.

This PDF file includes:

Sections S1 to S3

Figures S1 to S3

Movies S1 to S13

Supplementary Text

Section S1. Estimation of the blocking force F_b

To estimate the blocking force F_b, we model the soft manipulator as a planar elastica.[24] This model assumes that the manipulator body undergoes pure bending in a plane and the blocking force is perpendicular to the manipulator tip. We define a centerline curve $s \in [0, L]$, which passes through the centroid of all the cross sections of the manipulator body with an initial length L. Every point along this curve has a position $p \in R^2$ and a rotation $R \in R^{2\times 2}$, relative to a fixed frame at the base of the manipulator. Assuming the elastica is inextensible, the kinematics are given as (Fig. S1a):

$$R(s) = \begin{bmatrix} \cos(\theta) & -\sin(\theta) \\ \sin(\theta) & \cos(\theta) \end{bmatrix} \tag{S1}$$

$$\frac{dR}{ds} = R \begin{bmatrix} 0 & -\frac{d\theta}{ds} \\ \frac{d\theta}{ds} & 0 \end{bmatrix} \tag{S2}$$

$$\frac{d\boldsymbol{p}}{ds} = \begin{bmatrix} -\sin\theta(s) \\ \cos\theta(s) \end{bmatrix} \tag{S3}$$

Here, θ is the angle relative to the vertical axis at a given point s and $\frac{d\theta}{ds}$ is the angular strain of the manipulator body. Considering the statics of the manipulator, based on the moment balance at every point along the manipulator body, we have

$$EI\frac{d\theta}{ds} = M_{block}(s) + M_{act}(s) \tag{S4}$$

Here, E is the Young's modulus of the manipulator, I is the second moment of area for the manipulator cross section, M_{block} is the moment due to the blocking force, and M_{act} is the moment due to the TCA. The moment due to the blocking force M_{block}, which is due to an applied load F_b perpendicular to the tip of the manipulator, can be obtained by multiplying F_b with the distance along the manipulator body from the tip to the point at s,

$$M_{block} = F_b\left[\left(p_x(L) - p_x(s)\right)\sin(\alpha) + \left(p_y(L) - p_y(s)\right)\cos(\alpha)\right] \tag{S5}$$

Here, α is the bending angle at the tip of the manipulator (i.e., $\theta(L) = \alpha$, $p_x(s)$ and $p_y(s)$ are the two components of the position $\boldsymbol{p}(s)$, i.e., $\boldsymbol{p}(s) = \begin{bmatrix} p_x(s) \\ p_y(s) \end{bmatrix}$. Since the moments are not a function of θ, we can take the derivative of Equation S4 to get the moment balance to be dependent only on θ.

$$EI\frac{d^2\theta}{ds^2} = -F_b\cos(\theta - \alpha) + \frac{dM_{act}}{ds} \tag{S6}$$

The distributed moment due to the TCA is a subtle point, which is due to the change in the orientation of the TCA and is given as,

$$\frac{dM_{act}}{ds} = -F_{act}r\frac{d\theta}{ds} \tag{S7}$$

Here, r is the distance from the centerline to the manipulator. Therefore, Equation S6 can be re-written as,

$$EI\frac{d^2\theta}{ds^2} = -F_b\cos(\theta - \alpha) - F_{act}r\frac{d\theta}{ds} \tag{S8}$$

The boundary conditions include the fixed end at the manipulator base and the free end at the manipulator tip. At the fixed end of the manipulator, $\theta(0) = 0$, $p(0) = \begin{bmatrix} 0 & 0 \end{bmatrix}^T$, and $R(0) = \mathrm{diag}([1,1])$. At the free end of the manipulator, $\theta(L) = \alpha$ and $\frac{d\theta}{ds}(L) = 0$. The stiffness EI can be determined using the parallel axis theorem on both of the materials' cross sections (see Fig. S1b),

$$EI = E_1\left(I_{z,1} + A_1d_1^2\right) + E_2\left(I_{z,2} + A_2d_2^2\right) \tag{S9}$$

Here, $I_{z,i}$ is the second moment of area of the cross section, E_i is the Young's modulus, A_i is the area of the cross section, and d_i is the distance from the centerline to the center of the cross section for the softer (i = 1) and stiffer (i = 2) layers.

Since the static system of equations is a boundary value problem, we can use a shooting method to solve them numerically by making an initial guess of blocking force F_b and actuation force F_{act} that can be obtained using a physics-based model.[20] The shooting method works by wrapping an initial value problem solver (e.g., a Runge-Kutta integrator) in a root finding method, which solves for the unknown initial conditions (e.g., the blocking force) by repeatedly integrating the ODEs and checking that the boundary conditions are satisfied through the refinement of the guesses. For the statics, we know, $\theta(0)$ and $\frac{d\theta}{ds}(L)$ and need to have α to integrate the ODEs. So, we treat $\frac{d\theta}{ds}(0)$ and α as unknown initial conditions. Further, we specify two boundary conditions: the integrated value of $\theta(L)$ must match the guessed α and the calculated $\frac{d\theta}{ds}(0)$ must match the known tip condition, which gives us a fully constrained system. So, given the actuation and blocking forces, we can determine the shape of the manipulator (i.e., solve for $\boldsymbol{p}(s)$) using the shooting method. Subsequently, we approximate the bending curvature κ of the manipulator by taking the computed values of $\boldsymbol{p}$ and fitting a circle passing through three points of the manipulator: the base point $p_1 = \boldsymbol{p}(0)$, the middle point $p_2 = \boldsymbol{p}(L/2)$, and the tip point $p_3 = \boldsymbol{p}(L)$. Using the radius of the fitted circle, we can calculate the curvature as,

$$\kappa = \sqrt{\frac{4x_2^2\left(x_2y_3 - x_3y_3\right)^2}{\left(x_2^2 + y_2^2\right)\left(x_2^2y_3 - x_3^2y_2 + y_2^2y_3 - y_2y_3^2\right)^2}} \tag{S10}$$

Here, we have resolved p_2 and p_3 into their x and y components,

$$p_2 = \begin{bmatrix} p_x\left(\frac{L}{2}\right) \\ p_y\left(\frac{L}{2}\right) \end{bmatrix} = \begin{bmatrix} x_2 \\ y_2 \end{bmatrix},\ p_3 = \begin{bmatrix} p_x(L) \\ p_y(L) \end{bmatrix} = \begin{bmatrix} x_3 \\ y_3 \end{bmatrix} \tag{S11}$$

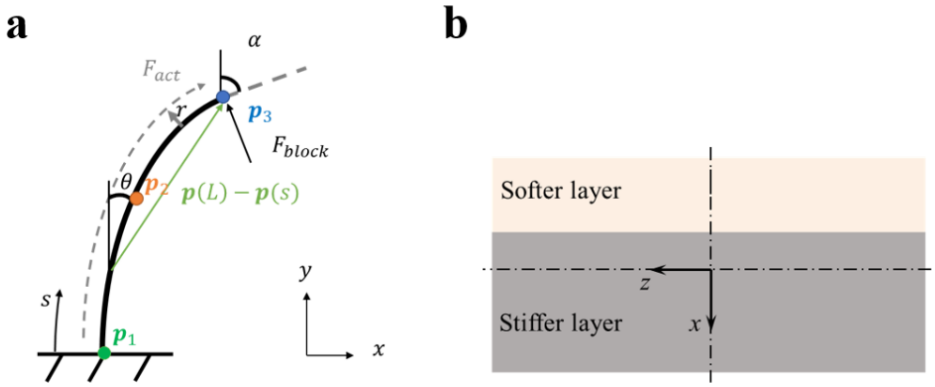

Figure S1. (**a**) Schematic illustrating the elastic model of soft manipulator. (**b**) Schematic illustrating the cross-section of the soft manipulator.

Section S2. Design of the manipulator for simultaneous droplet manipulation

The manipulator for simultaneous droplet manipulation consisted of a single heterochiral TCA in an elliptical shape, with the stiffer elastomer layer facing upward (Fig. S2), so that the two free ends of manipulator can bend upward simultaneously upon actuation.

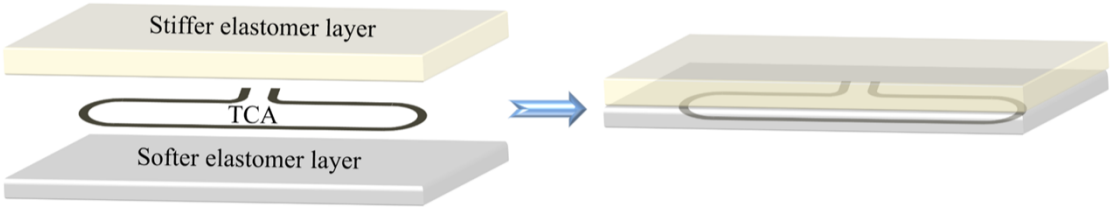

Figure S2. Schematic of the manipulator for simultaneous droplet manipulation.

Section S3. Lossless nature of droplet manipulation and cross-contamination on biofluid manipulators

We evaluated the lossless nature of droplet manipulation and cross-contamination on our biofluid manipulators by measuring the droplet volume, actuator mass and droplet roll off angle as a function of the droplet rastering cycles.

First, we measured the droplet volume and visually inspected the droplets as a function of droplet rastering cycles, sequentially with multiple liquids (hexadecane, water, Bradford reagent, BSA, milk, virus replicon particle laden solution, thrombin, whole blood, fibrinogen and PRP), on a single biofluid manipulator. In each cycle, a 30 µl pendant droplet of the desired liquid was rastered across the surface of the same biofluid manipulator using a linear translation stage. The droplet appearance was inspected, and the droplet image was captured after every 50 cycles and analyzed with ImageJ to determine the droplet volume. Even after 1000 droplet rastering cycles with each liquid, sequentially on the same manipulator, there is neither a significant change in the volume of any droplet (see Figure S3a) nor a discernible change in the appearance of any droplet. These results confirm that there is neither liquid loss nor noticeable cross-contamination associated with our droplet manipulations.

Second, we measured the manipulator mass and visually inspected the manipulator surface as a function of droplet rastering cycles, sequentially with multiple liquids (hexadecane, water, Bradford reagent, BSA, milk, virus replicon particle laden solution, thrombin, whole blood, fibrinogen and PRP), on a single biofluid manipulator. In each cycle, a 30 µl pendant droplet of the desired liquid was rastered across the surface of the same biofluid manipulator using a linear translation stage. The manipulator surface appearance was inspected, and the manipulator mass was measured after every 50 cycles. Even after 1000 droplet rastering cycles with each liquid,

sequentially on the same manipulator, there is neither a significant change in the manipulator mass (see Figure S3b) nor any change in manipulator surface appearance. These results also confirm that there is neither liquid loss nor noticeable cross-contamination associated with our droplet manipulations.

Third, we measured the roll off angles as a function of droplet rastering cycles, sequentially with multiple liquids (hexadecane, water, Bradford reagent, BSA, milk, virus replicon particle laden solution, thrombin, whole blood, fibrinogen and PRP), on a single biofluid manipulator. In each cycle, a 30 µl pendant droplet of the desired liquid was rastered across the surface of the same biofluid manipulator using a linear translation stage. The roll off angle of the liquid (which is very sensitive to surface inhomogeneity) was measured after every 50 cycles. Even after 1000 droplet rastering cycles with each liquid, sequentially on the same manipulator, there is no significant change in the roll off angle of any droplet (see Figure S3c). These results further confirm that there is neither liquid loss nor noticeable cross-contamination associated with our droplet manipulations.

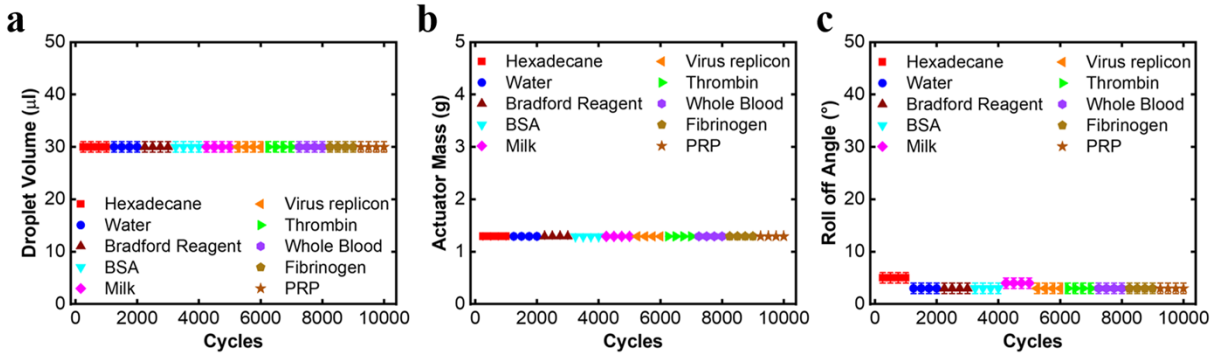

Figure S3. (**a**) Droplet volume as a function of droplet rastering cycles. (**b**) Actuator mass as a function of droplet rastering cycles. (**c**) Droplet roll off angle as a function of droplet rastering cycles.

Movie Legends

Movie S1

Demonstration of large bending angles and quick recovery of soft actuator upon actuation (2X speed).

Movie S2

Bouncing droplets of high and low surface tension liquids (water and hexadecane) on our superomniphobic surfaces (2X speed).

Movie S3

In-plane simultaneous mixing of water droplets (dyed red and blue) using our biofluid manipulator (2X speed).

Movie S4

In-plane simultaneous mixing of n-hexadecane droplets (colorless and dyed red) using our biofluid manipulator (2X speed).

Movie S5

In-plane sequential mixing of water droplets (dyed red, yellow and blue) using our biofluid manipulator.

Movie S6

Out-of-plane manipulation of water droplets (dyed yellow and blue) using our droplet gripper (4X speed).

Movie S7

Out-of-plane manipulation of n-hexadecane droplets (dyed red and colorless) using our droplet gripper (4X speed).

Movie S8

In-plane simultaneous droplet manipulation for protein detection with BSA and Bradford reagent using our biofluid manipulator.

Movie S9

In-plane simultaneous droplet manipulation for protein detection with milk and Bradford reagent using our biofluid manipulator.

Movie S10

In-plane simultaneous droplet manipulation for protein detection with virus-replicon particles and Bradford reagent using our biofluid manipulator.

Movie S11

In-plane simultaneous droplet manipulation for coagulation with whole blood and thrombin using our biofluid manipulator.

Movie S12

In-plane simultaneous droplet manipulation for coagulation with PRP and thrombin using our biofluid manipulator.

Movie S13

In-plane simultaneous droplet manipulation for coagulation with fibrinogen and thrombin using our biofluid manipulator.